LA-UR- 91-3167

LA-UR--91-3167

DE92 002415

TITLE: COMPARISONS OF COMPUTED AND MEASURED THREE-DIMENSIONAL VELOCITY FIELDS IN A MOTORED TWO-STROKE ENGINE

AUTHOR(S): Anthony A. Amsden, T-3
Peter J. O'Rourke, T-3
T. Daniel Butler, T-3
Keith Meintjes, General Motors Research Laboratories
Todd D. Fansler, General Motors Research Laboratories

SUBMITTED TO: 1992 SAE International Congress and Exposition, Detroit, Michigan, February 24-28, 1992

Los Alamos National Laboratory
Los Alamos, New Mexico 87545

FORM NO. 836 R4
ST. NO. 2629 5/81

COMPARISONS OF COMPUTED AND MEASURED THREE-DIMENSIONAL VELOCITY FIELDS IN A MOTORED TWO-STROKE ENGINE

Anthony A. Amsden, Peter J. O'Rourke, and T. Daniel Butler
Los Alamos National Laboratory, Los Alamos, NM

Keith Meintjes and Todd D. Fansler
General Motors Research Laboratories, Warren, MI

ABSTRACT

Computer simulations are compared with measurements of the three-dimensional, unsteady scavenging flows of a motored two-stroke engine. Laser Doppler velocimetry measurements were made on a modified Suzuki DT-85 ported engine. Calculations were performed using KIVA-3, a computer program that efficiently solves the intake and exhaust port flows along with those in the cylinder. Measured and computed cylinder pressures and velocities are compared. Pressures agree well over the cycle as do the velocities at the intake ports. In-cylinder velocities differ in detail, but the tumbling motion in the cylinder is well replicated in a vertical plane passing through the cylinder axis.

INTRODUCTION

Over the past several years, computational fluid dynamics (CFD) has been increasingly accepted as an adjunct to experimentation in the design and understanding of practical combustion systems. A major goal in the engine modeling effort, the calculation of three-dimensional engine flows with spray and combustion, was realized in 1987.[1,2] Since that time, three-dimensional studies with spray and/or combustion have become commonplace in the literature.[3-9] A recent patent for a high-turbulence piston design specifically identifies three-dimensional computer simulation for making the invention possible.[10]

Analyzing the scavenging flows of an operating two-stroke engine presents another opportunity for advancement in the sophistication and comprehensiveness of computational models and their associated verification experiments. This is a particularly challenging area in which experiment and modeling can play complementary roles in the design process, because the calculations can readily give information on scavenging that cannot be obtained experimentally. However, calculating these flows necessitates simultaneously solving for the flows in the connecting intake and exhaust channels as well as the cylinder. Flows in these channels strongly affect the scavenging process and cannot, in general, be supplied merely as boundary conditions to the in-cylinder flows. This paper presents the results of a combined theoretical and experimental study of a Suzuki DT-85 crankcase-compression, loop-scavenged, two-stroke engine operating in a motored (non-firing) mode. The purpose is to see how well

the computations replicate the experiment in a cylinder geometry modified to permit optical access.

The measurements give a quantitative picture of the air flow velocities and chamber pressures during the engine cycle. Ensemble-averaged velocities are measured by laser Doppler velocimetry (LDV) at up to 72 in-cylinder locations at 5° crank angle intervals and at 26 points on port-cylinder interfaces at 1° intervals. The crankcase, cylinder and exhaust pressures were recorded simultaneously at 0.5°-crank angle intervals.

The calculations were performed with KIVA-3[11], which solves the Navier-Stokes equations for three-dimensional compressible fluid flow supplemented by a two-equation turbulence model. The equations solved, their finite difference approximation, and the numerical solution procedure are the same as those of KIVA-II.[12,13] In particular, a standard version of the k-ε turbulence model is used, supplemented by volumetric expansion effects. Boundary layer drag and wall heat loss are calculated by matching to turbulent law-of-the-wall profiles.

KIVA-3 differs from KIVA-II in that it uses a block structured grid. The departure from a single rectangular structure in (i,j,k) logical space allows complex geometries to be modeled with significantly greater efficiency than was previously possible because large regions of deactivated cells are no longer necessary. A detailed description of KIVA-3 will be provided in a forthcoming report[11] that discusses the program features, the input required from a mesh generation code, and the output it provides to a graphics postprocessor.

We first describe the engine, its modifications, and the LDV instrumentation system used at General Motors Research Laboratories to map the flows responsible for the scavenging. Next we show the KIVA-3 computing mesh used in the simulations and discuss the computational parameters used in the program. The computed results are presented along side the experimental results, and the points of agreement and disagreement are discussed.

EXPERIMENT

Systematic laser-Doppler velocimetry measurements of the scavenging flow field were performed under motoring conditions both within the engine cylinder and at the intake-port-cylinder interfaces. The experimental apparatus and results are fully described in Ref.14, but a summary is included here for completeness.

Engine

The engine used here is a modified Suzuki DT-85 three-cylinder, two-stroke engine (see Table 1 for specifications). Fig. 1 shows a diametral cross section through the intake and exhaust ports (viewed from the head) together with a more detailed "unwrapped" drawing that indicates the port locations relative to the flat cylinder head used in these experiments. The engine employs one large exhaust port (denoted A in the sketch) and six smaller intake ports (B-G). The intake ports

and the transfer passages that connect them to the crankcase are *nominally* mirror-symmetric about an axial plane between the center of the exhaust port and the rib separating the two boost ports (D, E). This symmetry plane is offset 60° clockwise from the crankshaft axis. For the cylinder used in the LDV experiments, Table 2 lists the measured crank angles at which the ports are first uncovered and last covered by the top ring land and the piston face.

Table 1. DT-85 Engine Specifications

Number of cylinders	3
Displacement	1.2 L
Bore	84.0 mm
Stroke	72.0 mm
Connecting-rod length	135.9 mm
TDC clearance height	6.85 mm
Effective compression ratio	6.8

To provide optical access for LDV measurements, the original dished head of the cylinder located farthest from the flywheel was replaced by a flat quartz window mounted on a 6.35-mm spacer ring to maintain the proper clearance volume. The flat head simplifies the optics. The original domed piston was also machined flat, which may alter somewhat the angles of the flows entering the cylinder through the intake ports in the unmodified engine.

Table 2. DT-85 Port Timings (°ATDC)

Geometric Feature	Top Ring Land	Piston Face
Exhaust Port (A)		
Uncovered	85.0	90.0
Covered	275.0	270.0
Main (B,C,F,G) Ports :		
Uncovered	112.5	119.5
Covered	247.5	240.5
Boost Ports (D,E):		
Uncovered	116.0	123.5
Covered	244.0	236.5

Air was supplied to the engine from a critical-flow air system via a 4.75 L mixing tank, which permitted the air to be seeded with minute (~0.5 μm) silicone-oil droplets to serve as light scatterers for the LDV measurements. The stock carburetor was removed and the mixing tank connected to the crankcase intake by a long pipe.

Pressure pulsations in the exhaust system are important to the performance of two-stroke engines[15]. The pressure histories in motored and fired engines will differ greatly. This unavoidable difference will be reflected in the

behavior of the scavenging flows and must be kept in mind when interpreting the motored-engine flow-field results. Furthermore, preliminary LDV measurements and crude flow visualizations revealed that an unrealistically strong reverse flow into the cylinder occurred when the exhaust port is first uncovered. This backflow occurs because, when the engine is motored, the cylinder is already at about atmospheric pressure at exhaust-port opening, and the piston, being near mid-stroke, is moving at about its maximum speed, so that the cylinder volume increases rapidly and the cylinder pressure falls below the exhaust-manifold pressure. The resulting flow from the exhaust into the cylinder shortly before intake-port opening was sufficiently strong (~60-80 m/s at crank angle 115°ATDC) that it appeared likely to affect the flow field established by the intake process. The exhaust backflow was reduced to an acceptable level (<20 m/s at 115°) by isolating the exhaust port of the cylinder under study from the rest of the exhaust manifold and installing a reed valve in the exhaust pipe to restrict flow in the reverse direction. A side effect of this is that the cylinder pressure at intake-port opening is somewhat lower, and hence the intake velocities somewhat higher, than they would be in an unmodified, fired engine at the same delivery ratio.

Instrumentation

The photon-correlation LDV system and data-reduction procedures have been described in detail previously[16]; consult Ref. 14 Appendix A for additional information specific to this experiment.

The LDV measurement location (the intersection of the system's two focused laser beams) was positioned with about 0.1-mm accuracy by moving the entire optical system, which was rigidly mounted on a milling-machine base. LDV data within the engine cylinder were acquired along two orthogonal axes (one being the nominal symmetry axis of the port layout) at depths of 3, 26, 46 and 67 mm below the cylinder head. In some of the figures below, these diametral measurement planes are denoted as planes A, B, C and D, respectively. Plane A lies slightly above the midplane of the TDC clearance volume. Plane B is located midway between plane A and plane C, which is situated just above the top of the exhaust port. Plane D is slightly below the top of the main and auxiliary intake ports. Measurements of the flow through the intake-port faces were performed at various azimuthal locations at depths of 66 and 68 mm below the cylinder head, corresponding to distances of 1.65 and 3.65 mm below the top of the main and auxiliary ports.

In an auxiliary experiment, the crankcase, cylinder and exhaust pressures were recorded simultaneously at 0.5°-crank angle intervals (see Ref. 14, Appendix B). No modifications to the engine geometry or operating conditions used for the LDV measurements were made for the pressure measurements. Comparison of individual-cycle and ensemble-averaged pressure-crank-angle traces showed no statistically significant cycle-to-cycle variation.

Operating Conditions

The LDV measurements were performed under conditions appropriate to moderate speed, part-load operation of a passenger-car two-stroke engine, as indicated in Table 3. All the velocity data represent ensemble averages over many engine cycles.

Table 3. Experimental Operating Conditions

Engine speed (motored)	1600 rpm
Delivery ratio	0.52
Ensemble averages:	
No. cycles in ensemble	560 (intake ports) 900 (in cylinder)
Data-acceptance window width	1° (intake ports) 2° (in cylinder)
Window separation	1° (intake ports) 5° (in cylinder)

THE COMPUTER MODEL

The KIVA-II program[12,13] is in wide use for modeling chemically reacting flows with sprays in two- or three-space dimensions. KIVA-II lends itself well to confined in-cylinder flows and a variety of open combustion systems, but can become quite inefficient to use in complex geometries that contain such features as inlet ports and valves, diesel prechambers, and entire transfer ports. This is due to the large number of inactive cells that must be included in a KIVA-II calculation, as the computational domain must be encompassed by a single rectangular block of cells in (i,j,k) logical space. There is great interest in applying KIVA-II to the above complex geometries, however, as evidenced by the number of studies in which KIVA-II has been applied to complex flow domains in spite of the computational inefficiency.[17-20] The multiple-block structure of the KIVA-3 architecture offers a means of eliminating this inefficiency.

We now describe the KIVA-3 computational mesh and the parameters used in the numerical simulation engine experiment. Figure 2(a) shows several views of the complete mesh as it appears with the piston at BDC (bottom-dead-center, 180°). Note that in the cylinder our computational mesh does not correspond to a cylindrical coordinate system, but is instead derived from a non-periodic mapping of a single block of cells. Because it avoids the singularity associated with having a mesh axis, use of such a mesh for a cylinder requires fewer cells and allows larger timesteps when there are strong flows across the cylinder axis. The ports attached to this cylinder were created by processing coordinate data digitized from the actual ports, and asymmetries in the intake port geometries were accurately reproduced by the computational mesh. For the computer model, each of the three inflow ports consists of eight connected logical blocks of cells, and the exhaust port is a single block. The complete mesh is thus composed of 26 blocks,

which are then patched together into a single mesh for KIVA-3 by a preprocessor that also supplies the indices of cell neighbors, cell-face boundary condition definitions, and flags indicating active and inactive cells and vertices. The entire KIVA-3 mesh has 20,729 grid points. No provision in this mesh has been made to include the presence of the ring-crevice volume that exists in the experiments.

Contrast the plots in Fig. 2(a) with those of Fig. 2(b). This is the mesh configuration at TDC (top-dead-center, 0°) at the beginning and end of the calculation, when there are five completely disconnected regions. To move the piston from its TDC position to its BDC position and back again, special piston motion logic has been devised that differs from that of KIVA-II and that allows the connecting and disconnecting of port volumes with the in-cylinder volume. This logic, which we call SNAPPER, is now described.

The lowest plane of active cylinder vertices coincides with the piston face and moves in a Lagrangian fashion with the piston velocity. All other vertices remain stationary. Periodically, however, a new plane of piston-face vertices replaces the old plane and assumes its role of following the piston motion. An example with upward piston motion is shown schematically in Fig. 3. When the bottom row of cylinder cells has collapsed to some specified fraction of its original height, the bottom plane is deactivated and the next plane of vertices above assumes the role of the moving boundary. The old piston plane of vertices is "snapped" back to its original position, which is now below the piston face, and we perform a simple remap of the flow field onto the new mesh and redefine cell, vertex, and cell-face flags. When the piston is moving down the procedure is reversed and planes of cells are activated as the piston moves past them. Nothing special need be done when the piston moves past a port, and cell neighbor arrays need not be modified because mesh connectivity does not change. Our approach is limited to square ports and assumes that grid lines are horizontal around the periphery of the cylinder. Thus the rounded port openings of Fig. 1 are approximated by rectangles.

At the open boundaries of the intake and exhaust ports, we specify the experimentally measured crankcase and exhaust port pressures, respectively. These two values of applied pressure are updated each computational cycle by interpolating between experimental values supplied at 0.5° intervals. When flow exits these boundaries, the pressure specification is the only boundary condition needed. When flow enters a boundary, we flux in air that has the specified pressure and that is isentropically related to a reference state of one atmosphere and 325 K. In some earlier calculations, flow reversal at the exhaust port exit was prohibited to mimic the reed valve used in the cold flow experiment. We obtain better agreement with experimentally measured pressures, however, when we allow flow to enter the exhaust port boundary. We reason that the effects of the reed valve are already included in the imposed exhaust port pressure and that the computational results imply flow is bypassing the reed valve at some times in the experiment.

All calculations are begun at TDC, at which point all initial air is isentropically related to the reference state and, depending on its location, has the

experimentally measured cylinder, intake port, or exhaust port pressure. It is preferable to begin the calculation at TDC because our assumption of a null velocity field as an initial condition is more valid at TDC than at any other time. The wall temperatures are maintained at 325 K. Calculations are run two complete engine revolutions, and the calculated cylinder pressure and trapped mass are nearly the same at 360° and at 720°. Each complete engine revolution requires approximately 900 computational cycles and 1.6 hours on a Cray Y-MP operating in single processor mode.

COMPARISON OF EXPERIMENTS AND COMPUTATIONS

In this section we compare computed and measured cylinder pressures, delivery ratio, and ensemble-averaged velocities. Figure 4(a) gives the experimentally measured crankcase and exhaust pressures. After the intake ports open and the crankcase and cylinder pressures nearly equilibrate, the experimental crankcase and exhaust pressures oscillate out of phase with each other. Figure 4(b) gives the measured and calculated cylinder pressures over a 720° period. In the calculation, the top of the exhaust port was 44.7 mm below the cylinder head, compared to 47.9 mm in the experiment. This resulted in the calculated exhaust port opening at 86° ATDC, which closely corresponds to the experimental ring opening crank angle. Other calculations indicated a large sensitivity of the TDC pressure to the position of the top of the exhaust port. The higher the top of the exhaust port is, the earlier it is opened by the downward piston motion. The 86° timing gives the best agreement with the experimentally measured TDC pressure because, as has been noted in the section describing the experiment, communication between the port and the cylinder starts as soon as the top ring passes. Figure 4(c) is a close-up of the measured and calculated cylinder pressure during the time period when the exhaust port is open. Oscillations seen in the calculated cylinder pressures agree well with the frequency and amplitudes in the experiment.

The delivery ratio is defined to be the mass of air delivered to the cylinder through the inflow ports, divided by the density of dry air at standard temperature and pressure and divided by the volume displaced by the cylinder. The experimentally measured delivery ratio is 0.52, contrasted to 0.63 for the first 360° and 0.59 for the period 360°-720°. Although the calculated delivery ratio varies over the two engine cycles, very little difference is noted in the calculated velocity fields at the same corresponding crank angles while the ports are open. We attribute the difference primarily to slightly higher computed cylinder pressures during the second engine cycle. Nevertheless, the calculated delivery ratio is greater than the measured value. This difference may result from the approximations used for the port shapes and sizes in the calculations. The squaring of the cross-sections of the ports in the mesh and the exhaust port opening necessary to effect the 86° opening time yield larger openings and thus larger delivery ratios.

A particularly valuable part of the calculations is the ease with which the time history of the scavenging can be obtained. Figure 5 presents the mass of old and new air in the cylinder as a function of crank angle during the time the ports

are open. The purging of the old air from the cylinder is approximately linear from 130° - 270°. Most of the new air is supplied during the period from 120° to 150°. During this period the flow is filling the expanding cylinder volume with only a minor portion of old air exiting through the exhaust. After the first calculated cycle of operation, new air makes up 54% of the trapped mass after the ports are closed. The rest of the new air is short-circuited to the exhaust with a minor portion to the intake port channels.

We now compare experimentally measured velocities with computed velocities. Figures 6(a) - (i) give comparisons of in-cylinder velocities at crank angles of 115°, 125°, 135°, 150°, 180°, 260°, 295°, 330° and 360° ATDC. Figures 7(a) - (d) give comparisons of velocities in planes of the intake ports/cylinder interface at 130°, 135°, 140° and 150° ATDC. Only the computed velocities at the experimental measurement locations are shown in the figures.

We do not attempt here to quantify the differences between experiment and calculation, but we make some observations concerning general areas of agreement and disagreement. First, the agreement in Figs. 6(a)-(i) gets better as we move away from the exhaust port opening time. At 115° both the experiment and the calculation show flow entering the cylinder from the exhaust in the plane C, just above the top of the experimental exhaust port. This plane is anomalous because of the aforementioned differences in the calculated and experimental exhaust port height. Plane C in the calculations is below the top of the exhaust port. Even so, reverse flow persists longer in the calculation than in the experiment, as can be seen in the plots at 125°. Also at 125°, the effect of the boost port ring opening is especially pronounced in the measurements taken in the nominal symmetry plane. The piston face has not yet opened that port in the calculations. At 135° the upward flow in the symmetry plane, which is caused by the convergence of the intake flows, is considerably stronger in the calculation than in the experiment. The measured asymmetry is very pronounced as evidenced by the highly complex flow in plane C. At 150° the experimental velocities in the symmetry plane show a tumbling motion that begins to establish itself in the computed flow field. From 180° onward, the experimental tumbling motion is well reproduced by the calculation, as are the velocities in all other planes with the exception of a small residual swirl left in the measured velocity field at 360°.

In general, there is more asymmetry in the experimental velocity fields of Figs. 6(a)-(i) than in the calculated ones. The symmetry of the computed flow field is obtained despite the fact that asymmetries in the intake port geometries are represented with the computational mesh. Such asymmetry would result if, instead of applying a single crankcase pressure, different pressures pertained at the crankcase boundaries of the intake ports. Figures 7(a)-(c) show a fair degree of symmetry in the experimental velocities entering the cylinder from the side ports, but Fig. 7(d) shows some asymmetry that is not seen in the calculation and that could be the result of unequal pressures.

The computed velocities entering the side ports in Figs. 7(a)-(c) agree well with the experimentally measured values. Not shown in these figures is the tilt angle of the flow through the ports. The calculated tilt angles agree well with the observations of approximately 30° in the main and auxiliary ports and approximately 45° in the boost port measured near the midspan of the ports. We note, however, that although the calculated flow from the auxiliary and main ports is tilted upwards at the port, it turns downward upon entry to follow the piston. In Fig. 7(d), as has been observed above, there is some asymmetry in the experimental velocities that is not reproduced in the calculation. The calculations show cylinder flow into the boost port while the experiments show cylinder flow into a portion of the boost port and into an auxiliary port at 150°. In general the calculated velocities entering the boost port are smaller than the experimentally measured values, which could again be caused if a different pressure pertained at the crankcase boundary of the boost port than at the corresponding boundaries of the side ports. Since flow from the boost port is instrumental in causing the tumbling motion seen in the symmetry plane plots, some of the disagreement between the calculated and measured tumbling motion is probably caused by the reduced boost port flow in the calculation.

CONCLUSIONS

This paper shows detailed comparisons of computed results with measurements of the three-dimensional, unsteady scavenging flows of a motored two-stroke engine. Laser Doppler velocimetry measurements were made on a modified Suzuki DT-85 ported engine. Calculations were performed using KIVA-3, a computer program that efficiently solves the intake and exhaust port flows along with those in the cylinder. Measured and computed cylinder pressures and velocities are compared. Pressures agree well over the cycle as do the velocities at the intake ports. In-cylinder velocities differ in detail, but the tumbling motion in the cylinder is well replicated in the symmetry plane of the cylinder. The calculated delivery ratio is 14% greater than the measured value at these operating conditions.

Some of the largest differences between measured and calculated velocity fields occur during the initial period of port openings on the downward stroke of the engine. Probable causes for these differences are that despite the obvious complexity of the computing mesh used, an even more complex one is needed, one which accounts for rounded port corners and ring-crevice volumes. This latter particularly affects the communication timing between the ports and the cylinder. Further, asymmetries in the measured velocity field suggest that spatially varying conditions are present in the crankcase, resulting in a different pressure history for each intake opening.

ACKNOWLEDGMENTS

We are grateful to Margaret S. Fairfield for creating the video of the KIVA-3 calculation, which will be shown during the oral presentation. The work at Los Alamos National Laboratory is supported by the United States Department of Energy, Conservation and Renewable Energy, Advanced Industrial Concepts Division.

REFERENCES

1. F. Grasso, M. J. Wey, F. V. Bracco, and J. Abraham, "Three Dimensional Computations of Flows in a Stratified-Charge Rotary Engine," SAE Technical Paper 870409 (1987).

2. P. J. O'Rourke and A. A. Amsden, "Three-Dimensional Numerical Simulations of the UPS-292 Stratified Charge Engine," SAE Technical Paper 870597 (1987).

3. D. Gilaber and P. Pinchon, "Measurements and Multidimensional Modeling of Gas-Wall Heat Transfer in a S. I. Engine," SAE Technical Paper 880516 (1988).

4. J. D. Naber and R. D. Reitz, "Modeling Engine Spray/Wall Impingement," SAE Technical Paper 880107 (1988).

5. T. W. Kuo and R. D. Reitz, "Computation of Premixed-Charge Combustion in Pancake and Pent-Roof Engines," SAE Technical Paper 890670 (1989).

6. Y. Takenaka, Y. Aoyagi, Y. Tsuji, and I. Joko, "3D Numerical Simulation of Fuel Injection and Combustion Phenomena in DI Diesel Engines," SAE Technical Paper 890668 (1989).

7. R. D. Reitz and T. W. Kuo, "Modeling of HC Emissions Due to Crevice Flows in Premixed-Charge Engines," SAE Technical Paper 892085 (1989).

8. K. Naitoh, H. Fujii, T. Urushihara, Y. Takagi, and K. Kuwahara, "Numerical Simulation of the Detailed Flow in Engine Ports and Cylinders," SAE Technical Paper 900256 (1990).

9. W. K. Cheng and J. A. Diringer, "Numerical Modeling of SI Engine Combustion with a Flame Sheet Model," SAE Technical Paper 910268 (1991).

10. United States Patent No. 4,955,338, Diwakar et al (1990).

11. A. A. Amsden, P. J. O'Rourke, and T. D. Butler, "KIVA-3: A Block-Structured-Mesh KIVA Program for Complex Geometries," Los Alamos National Laboratory report, in preparation.

12. A. A. Amsden, T. D. Butler and P. J. O'Rourke, "The KIVA-II Computer Program for Transient Multidimensional Chemically Reactive Flows with Sprays," SAE Technical Paper 872072 (1987).

13. A. A. Amsden, P. J. O'Rourke, and T. D. Butler, "KIVA-II: A Computer Program for Chemically Reactive Flows with Sprays," Los Alamos National Laboratory report LA-11560-MS (1989).

14. T. D. Fansler and D. T. French, "The Scavenging Flow Field in a Crankcase-Compression Two Stroke Cycle Engine — A Three-Dimensional Laser-Velocimetry Survey," SAE Paper 92xxxx, 1992.

15. G. P. Blair, The Basic Design of Two-Stroke Engines," SAE, Warrendale, PA, 1990

16. T. D. Fansler, "Photon-Correlation Laser Velocimetry in Reciprocating-Engine Research." In J. B. Abbiss and A. E. Smart, editors, *Photon Correlation Techniques and Applications,* Opt. Soc. Amer. Conf. Proc. Ser., Vol. 1, 1988.

17. R. Taghavi and A. Dupont, "Multidimensional Flow Modeling," Cray Channels (10) 4 (1989), p.18.

18. M. Zellat, Th. Rolland, and F. Poplow, "Three Dimensional Modeling of Combustion and Soot Formation in an Indirect Injection Diesel Engine," SAE Technical Paper 900254 (1990).

19. P. Epstein, "A Computer Simulation of the Scavenging Flow in a Two-Stroke Engine," MSME Thesis, University of Wisconsin - Madison (1990).

20. P. H. Epstein, R. D. Reitz, and D. E. Foster, "Computations of a Two-Stroke Engine Cylinder and Port Scavenging Flows," SAE Technical Paper 910672 (1991).

Figure Captions

Fig. 1 Schematic drawing of the modified Suzuki DT-85 engine, showing a diametral cross-section through the ports and "unwrapped" cylinder indicating the port locations.

Fig. 2 The KIVA-3 computing mesh with the piston at (a) 180° and (b) 0°.

Fig. 3 Schematic showing the steps in the "snapper" procedure for mesh reconnection at the cylinder-port interface.

Fig. 4 (a) Experimental values of crankcase and exhaust pressure.
(b) Experimental and calculated cylinder pressures over two engine cycles.
(c) Close-up of the measured and calculated cylinder pressure.

Fig. 5 Calculated old and new air mass in the cylinder.

Fig. 6 Measured (left) and calculated (right) velocities at specified crank angles. The vertical viewing plane is through the nominal symmetry axis of the cylinder. The horizontal planes are identified in the figures and the text.

Fig. 7 Measured (left) and calculated (right) velocities at the port-cylinder interfaces at the indicated crank angles and distance from the head.

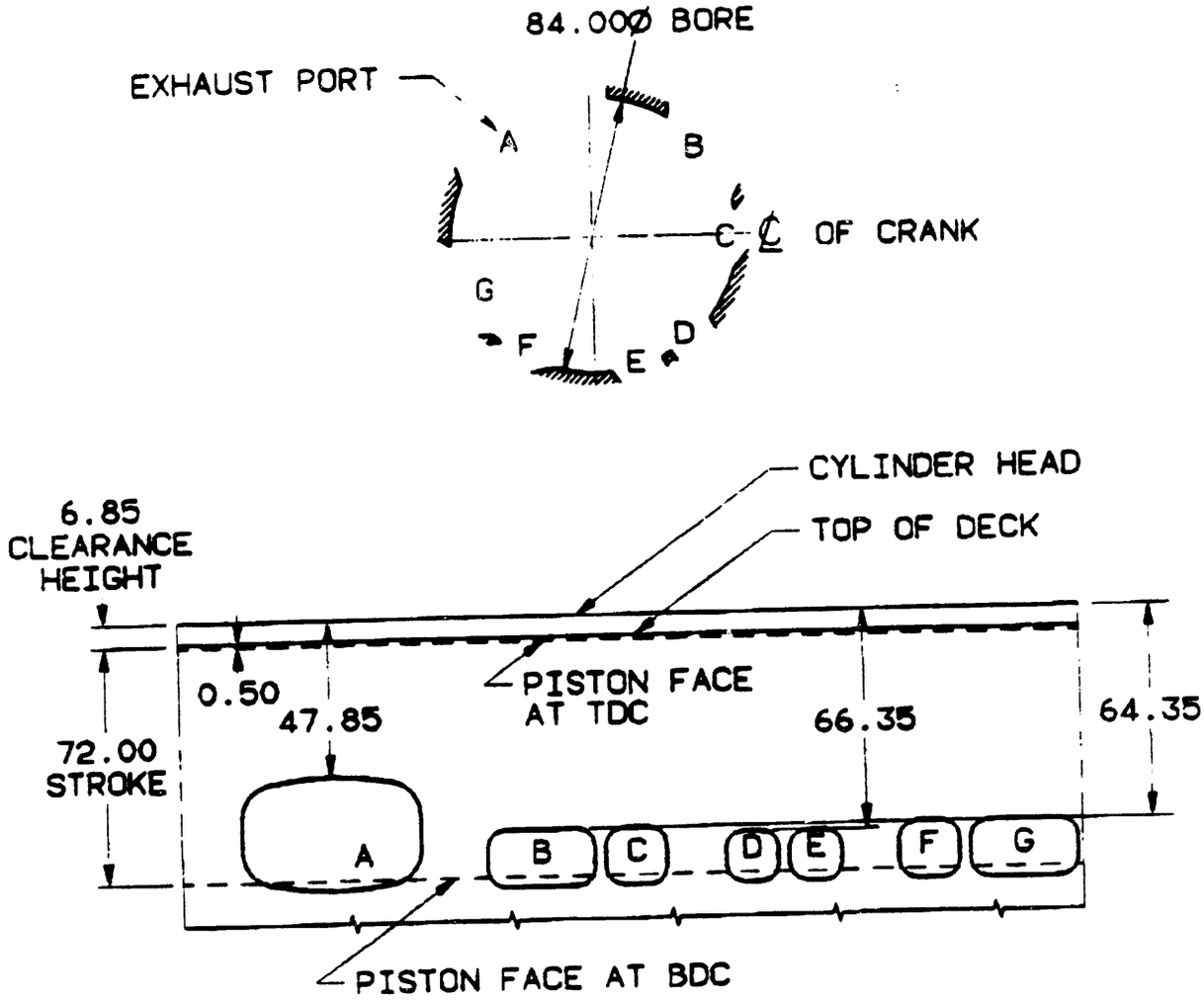
84.00Ø BORE
EXHAUST PORT
A
B
℄ OF CRANK
G
F
E
D
CYLINDER HEAD
TOP OF DECK
6.85
CLEARANCE
HEIGHT
0.50
47.85
PISTON FACE
AT TDC
66.35
64.35
72.00
STROKE
A
B
C
D
E
F
G
PISTON FACE AT BDC

Fig. 1

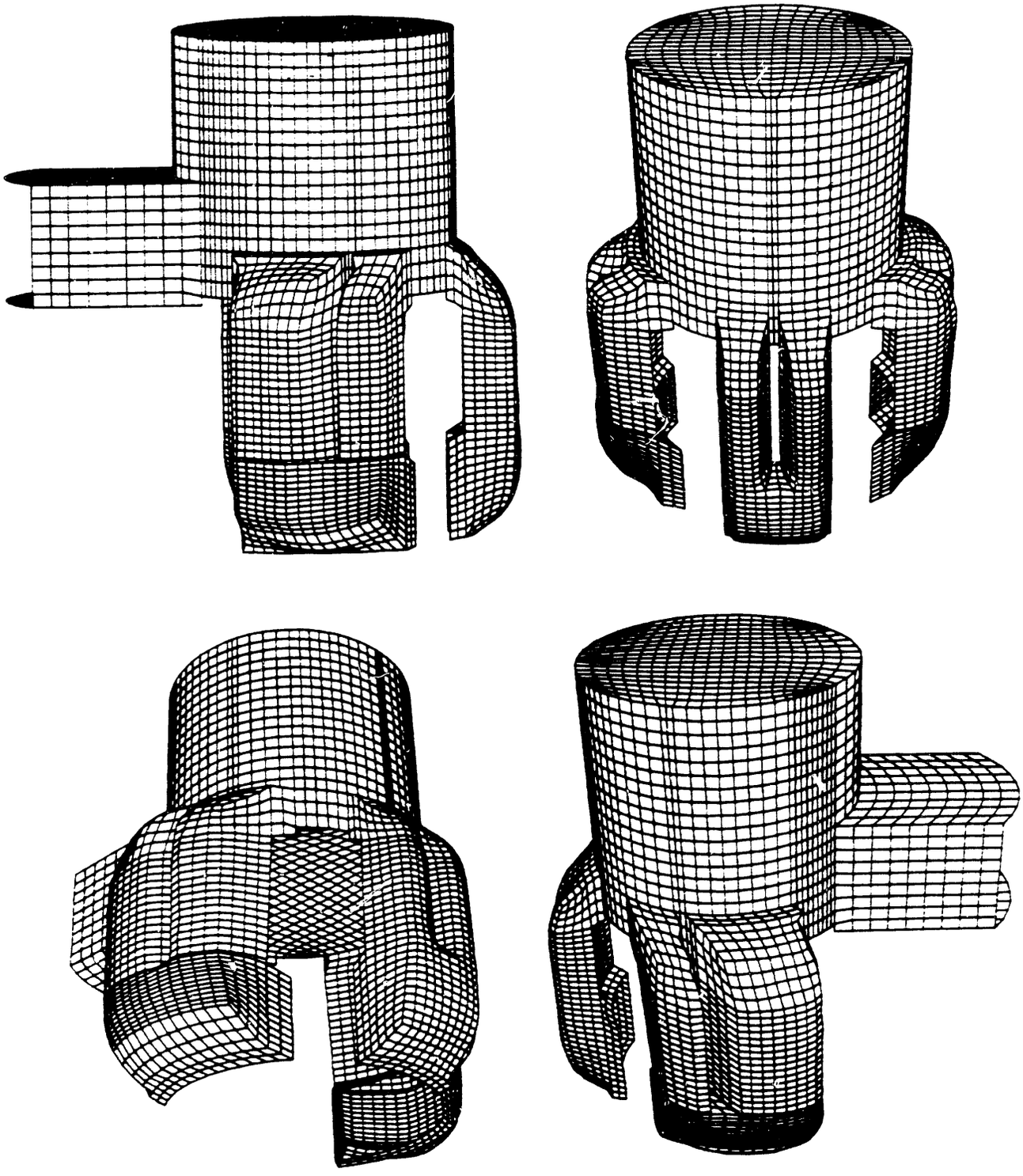

Fig. 2a

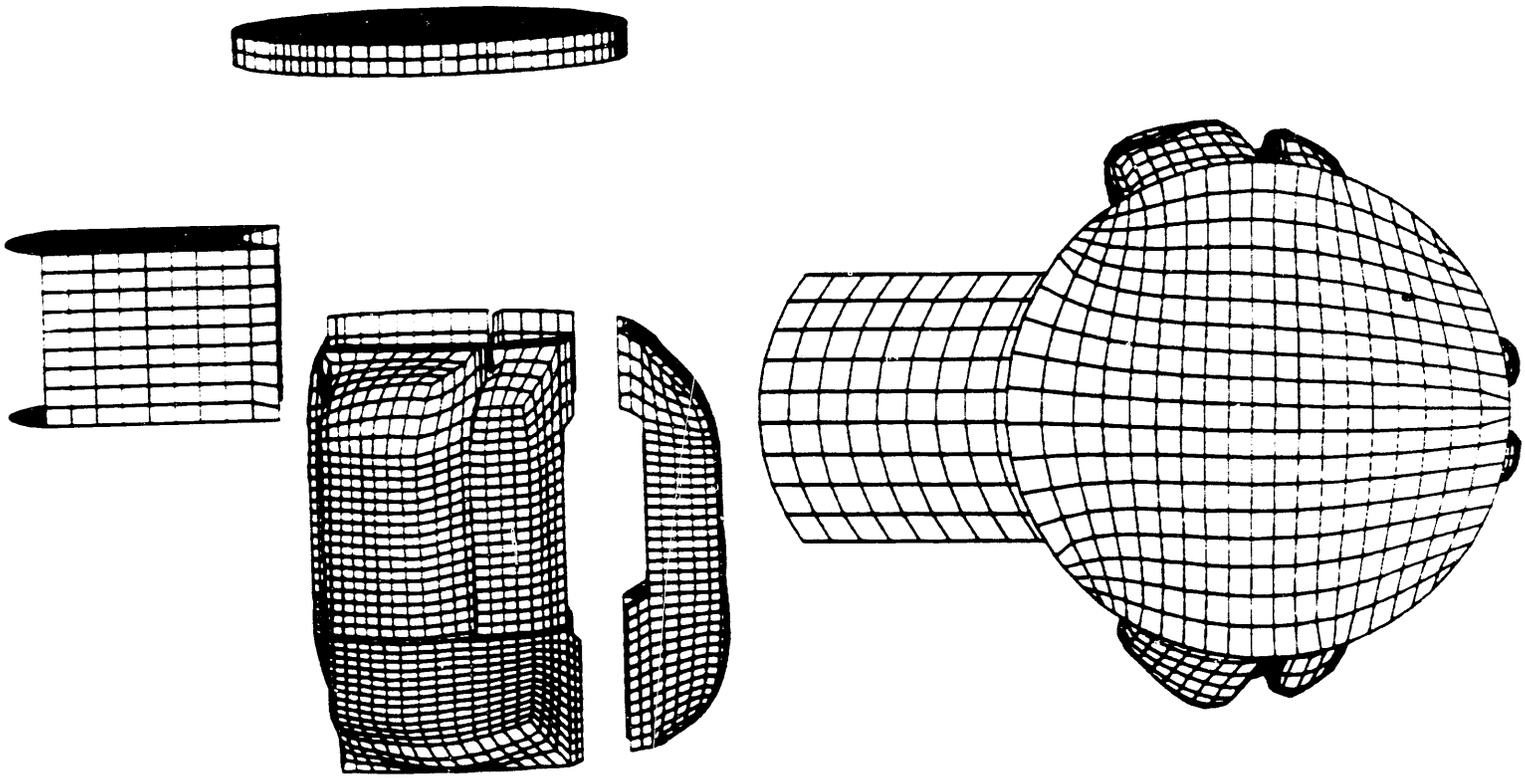

Fig. 2b

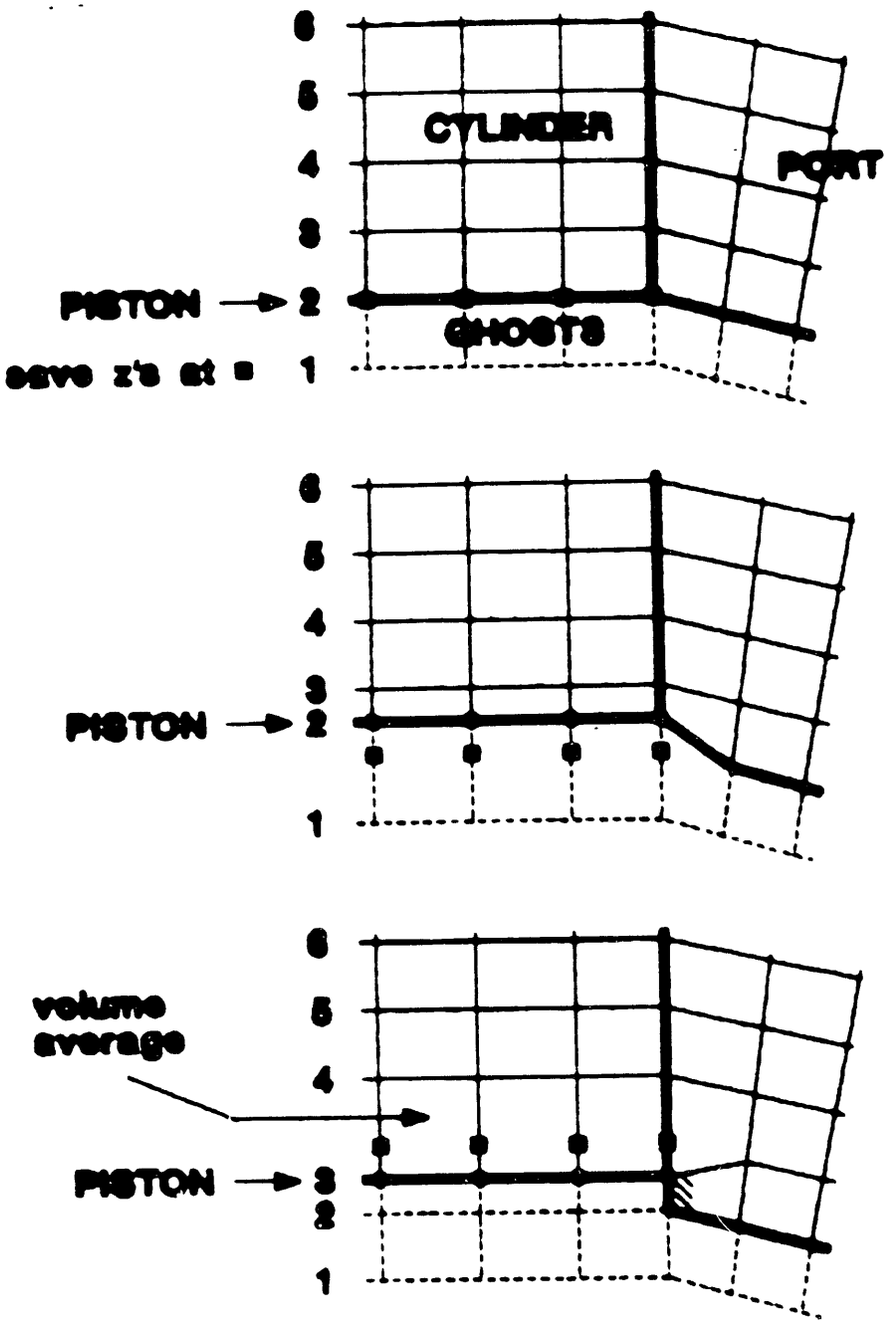
6
5
CYLINDER
4
PORT
3
PISTON
2
GHOSTS
1
6
5
4
3
PISTON
2
1
volume
average
6
5
4
PISTON
3
2
1

Fig. 3

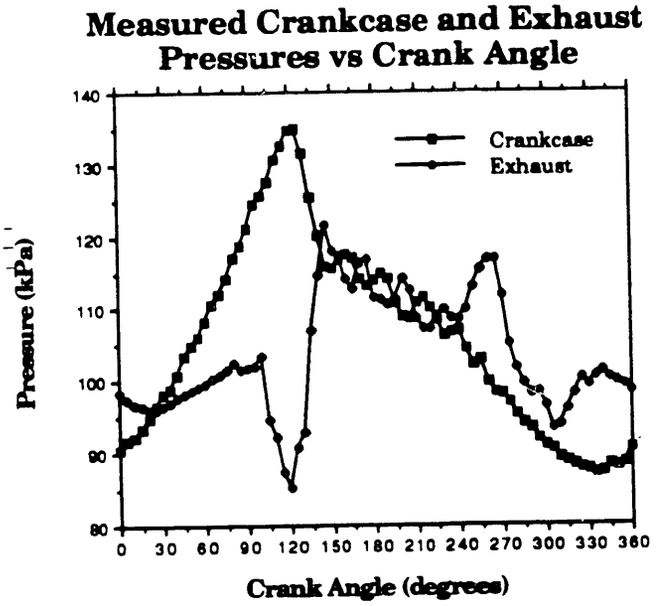

Fig. 4a

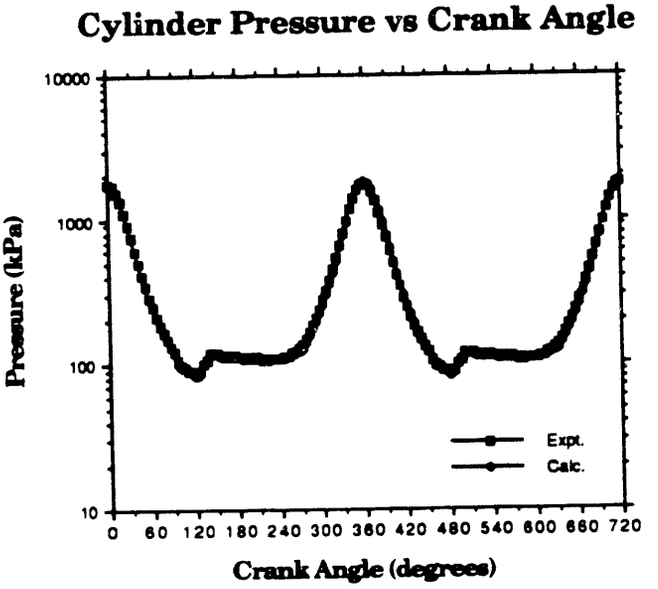

Fig. 4b

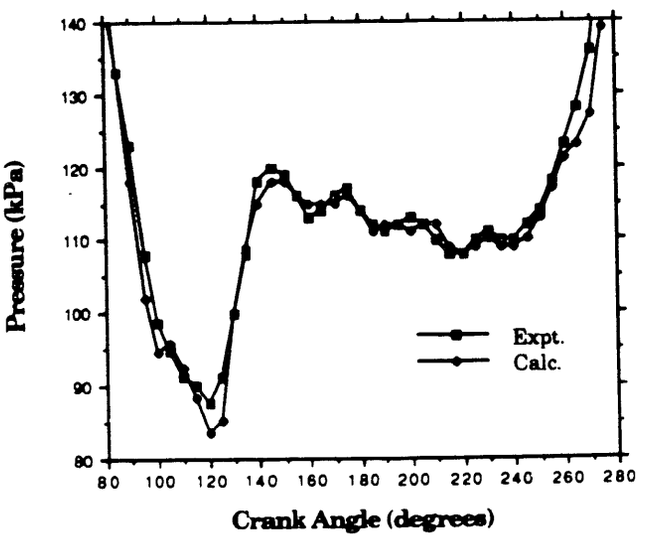

Fig. 4c

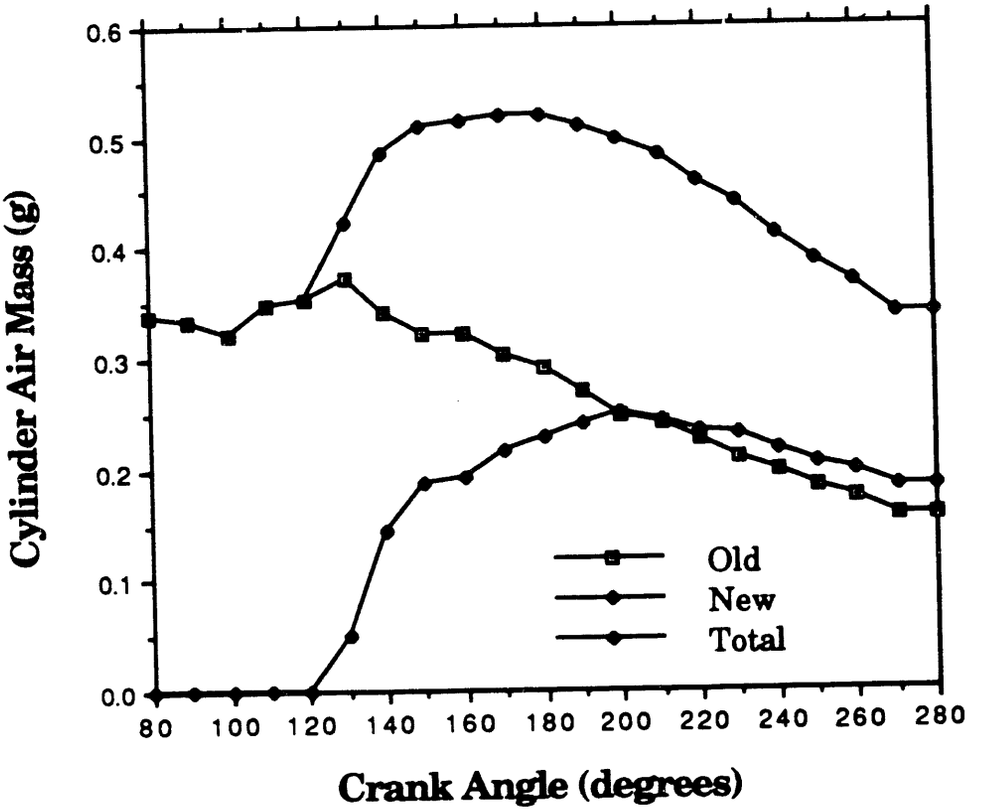
Cylinder Air Mass vs. Crank Angle
Cylinder Air Mass (g)
0.6
0.5
0.4
0.3
0.2
0.1
0.0
80
100
120
140
160
180
200
220
240
260
280
Crank Angle (degrees)
Old
New
Total

Fig. 5

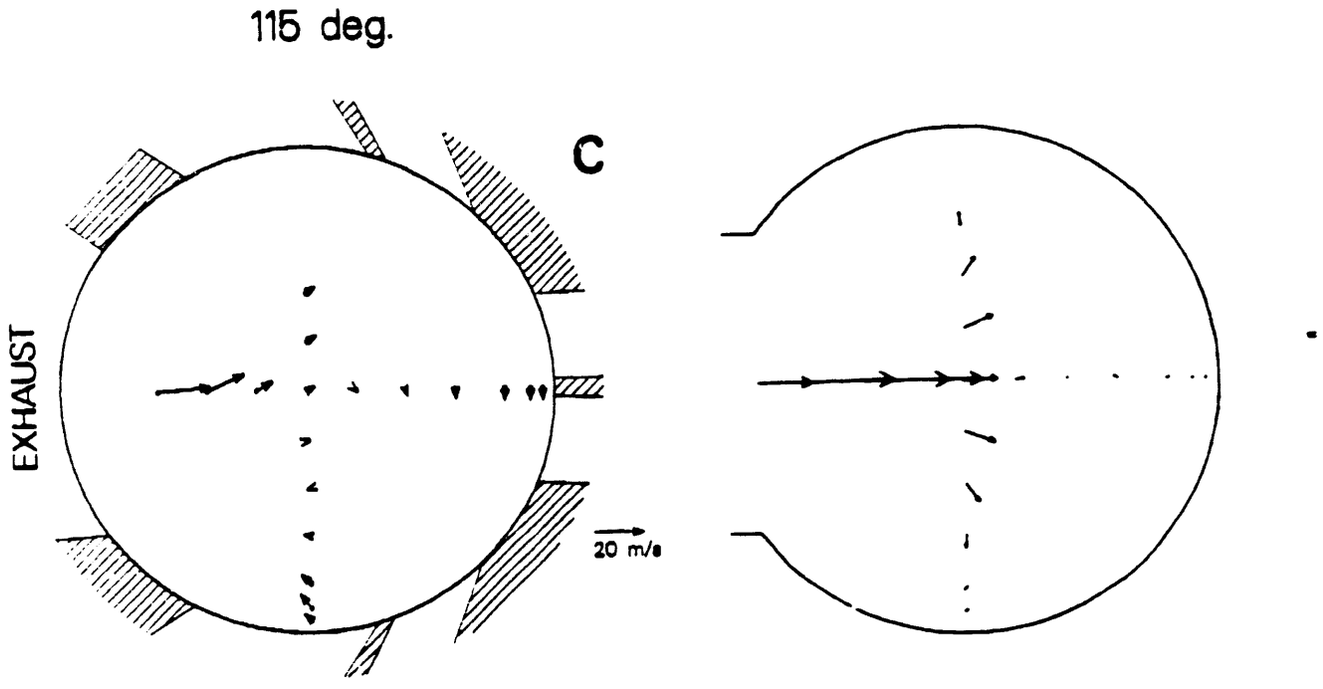

Fig. 6a

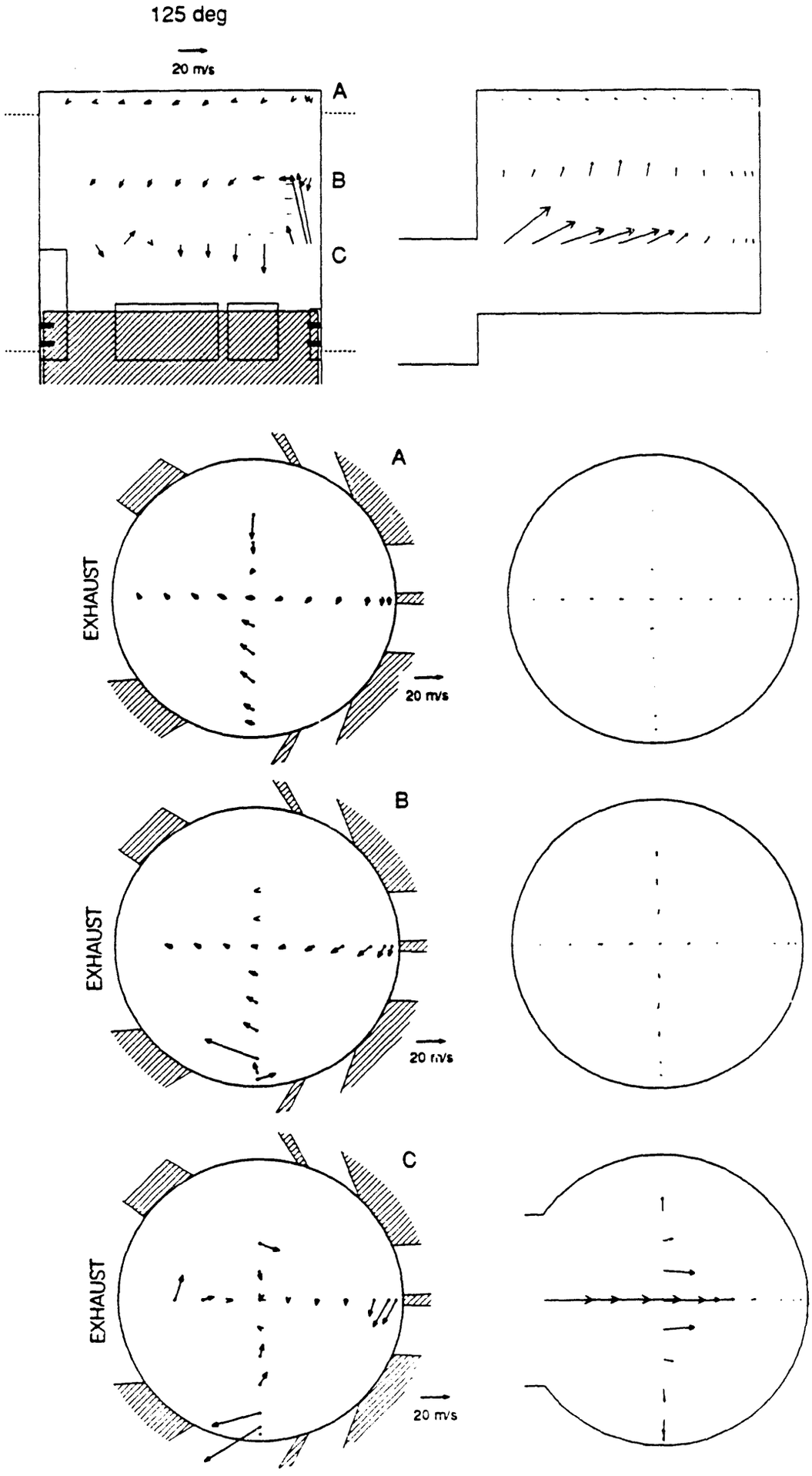

Fig. 6b

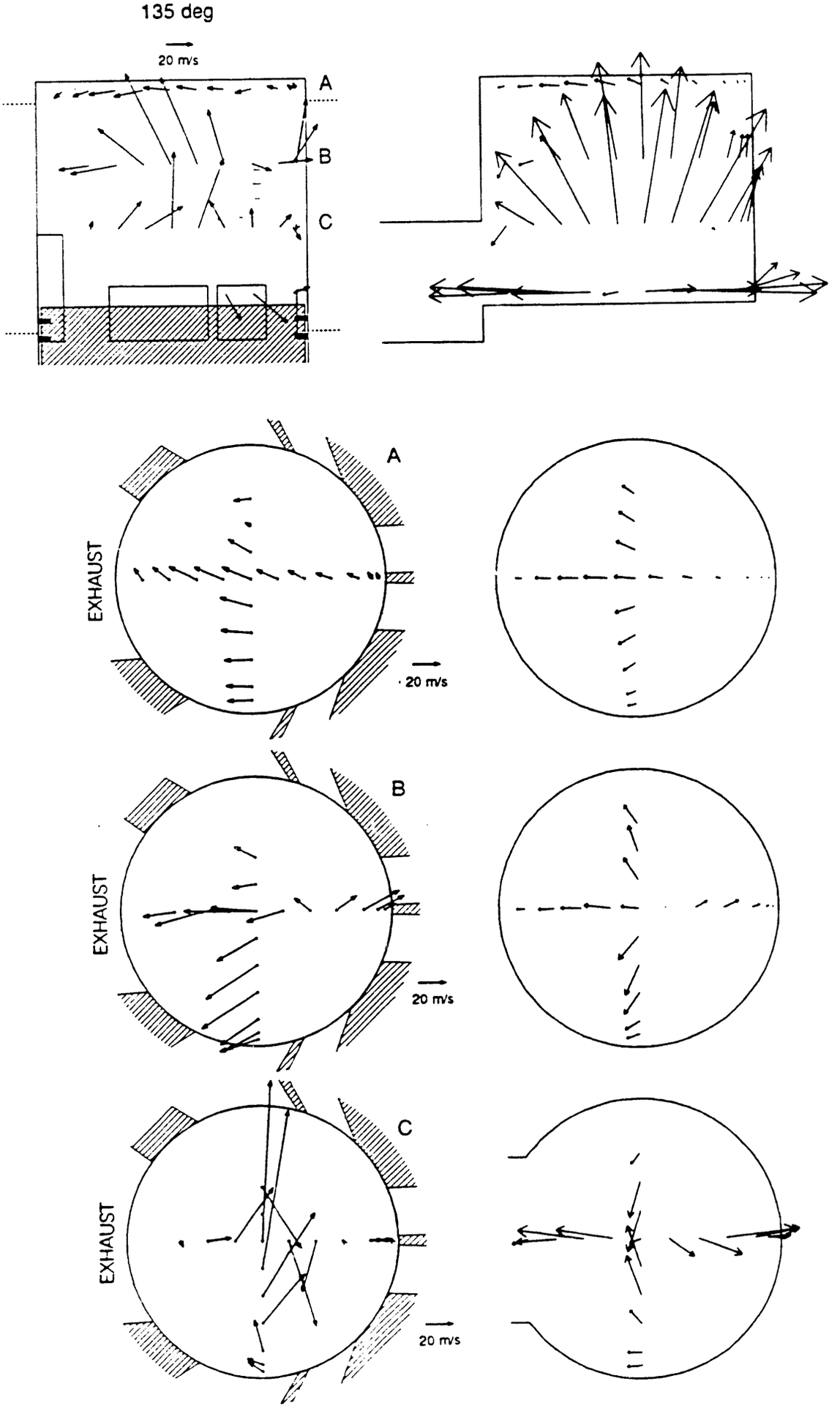
135 deg
20 m/s
A
B
C
EXHAUST
20 m/s
A
EXHAUST
20 m/s
B
EXHAUST
20 m/s
C
EXHAUST

Fig. 6c

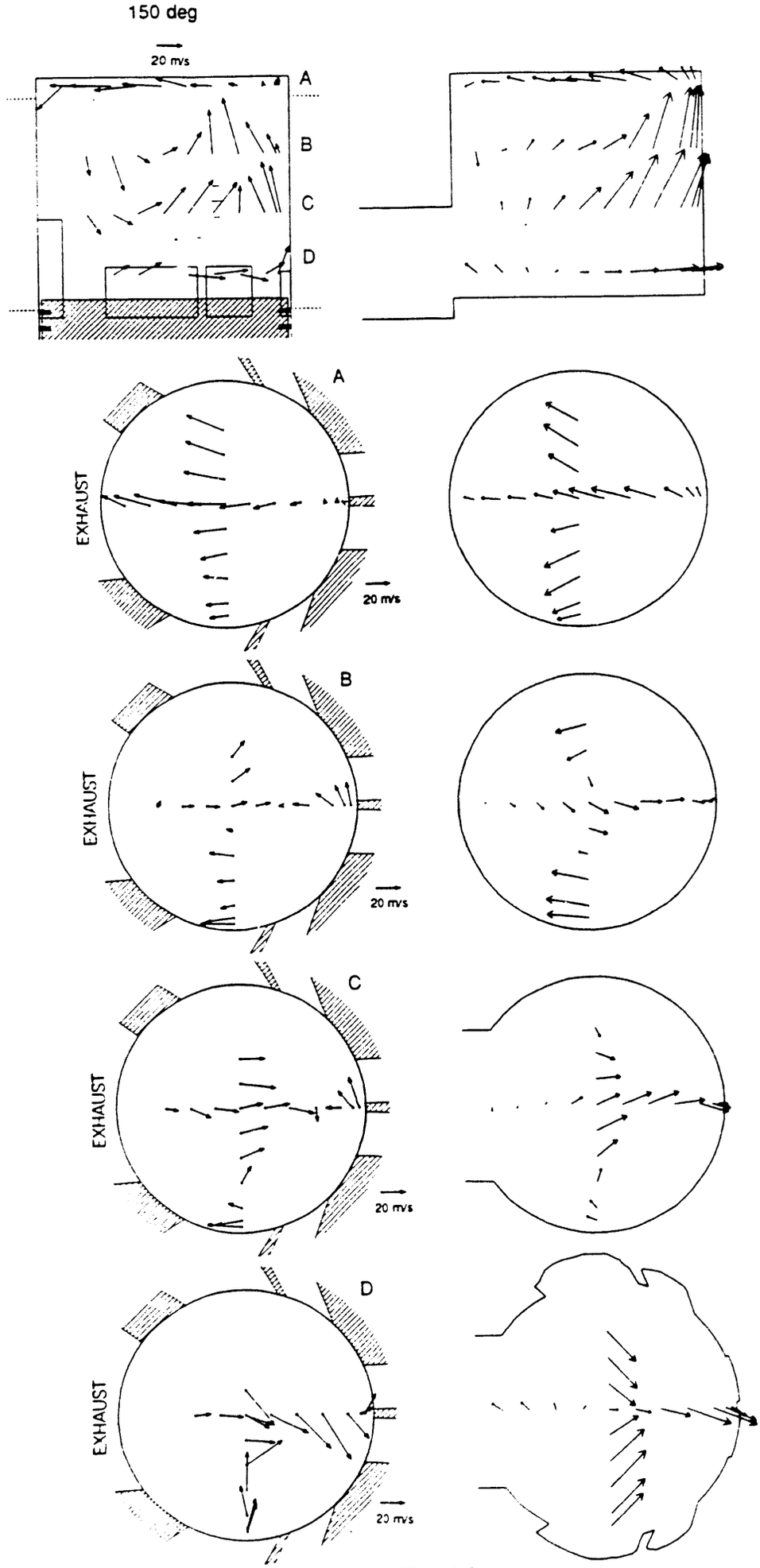

Fig. 6d

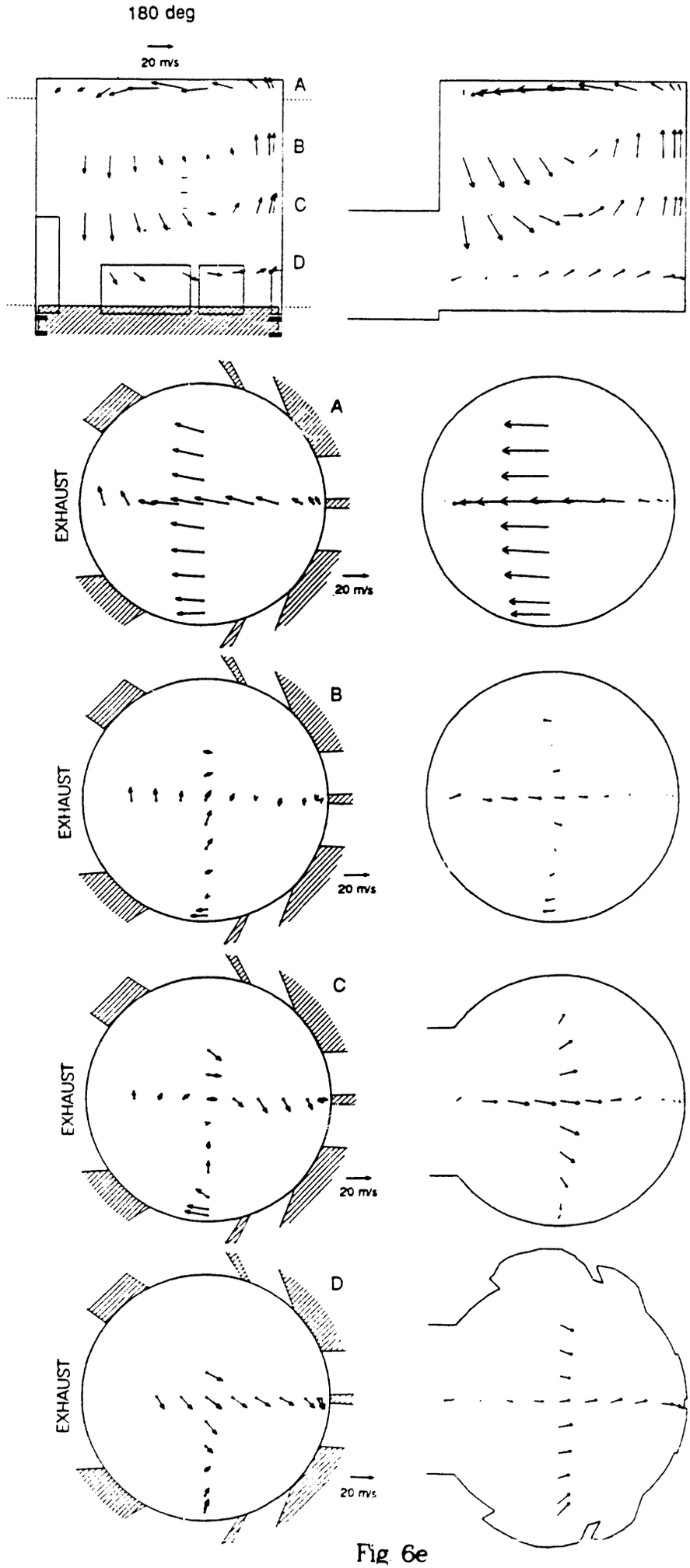

Fig. 6e

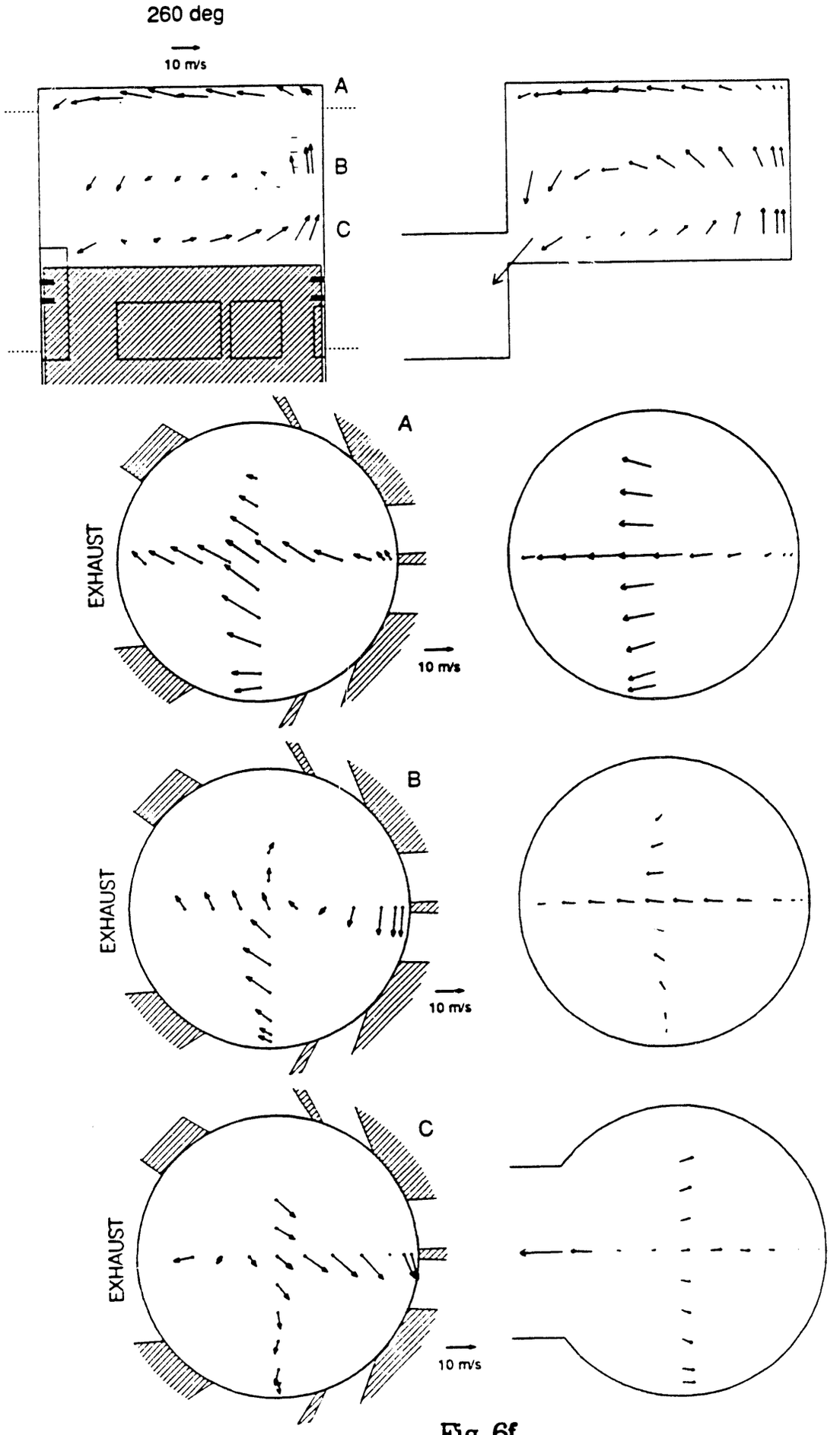
260 deg
10 m/s
A
B
C
EXHAUST
10 m/s
A
EXHAUST
10 m/s
B
EXHAUST
10 m/s
C
EXHAUST
10 m/s

Fig. 6f

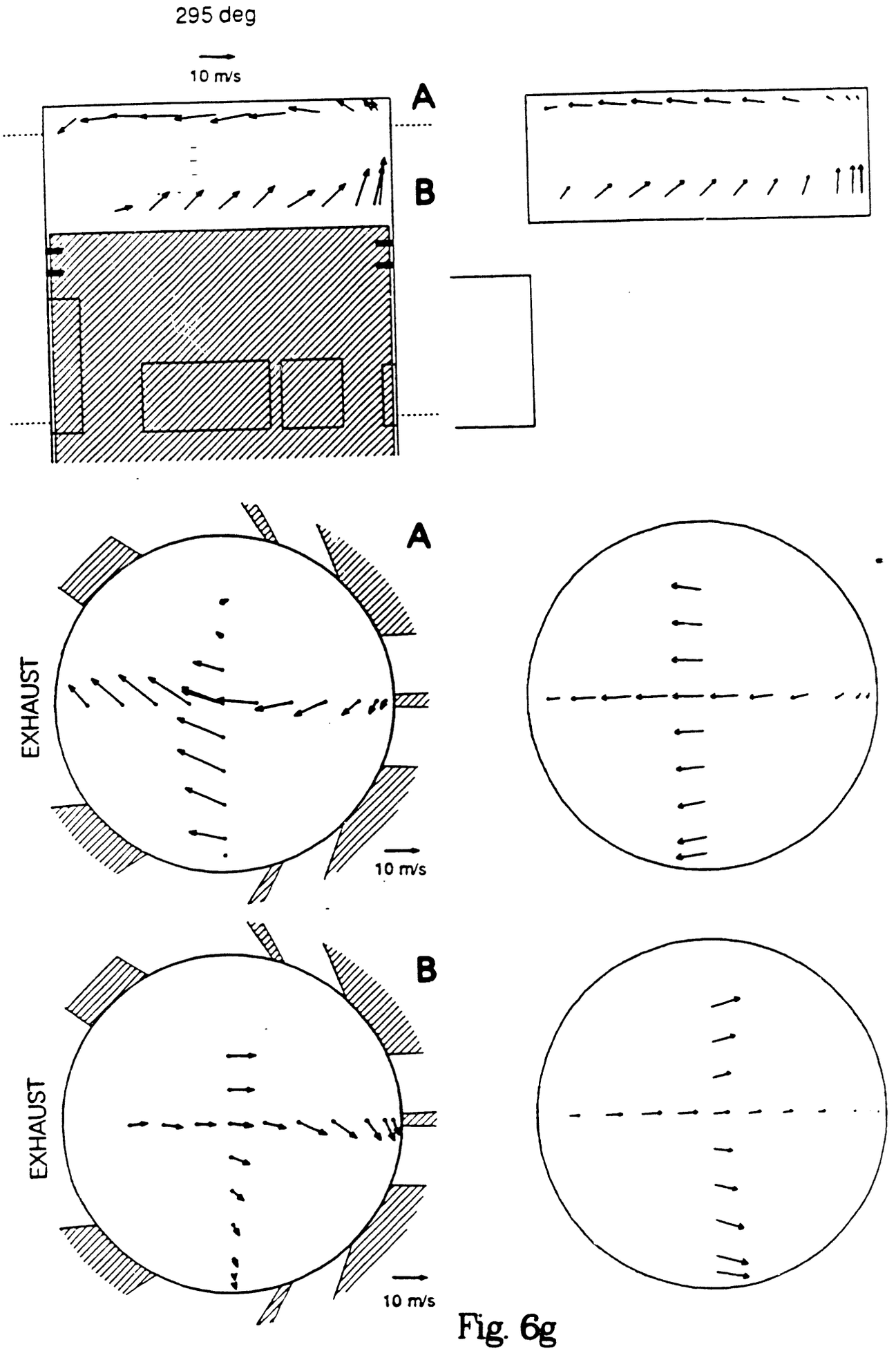

Fig. 6g

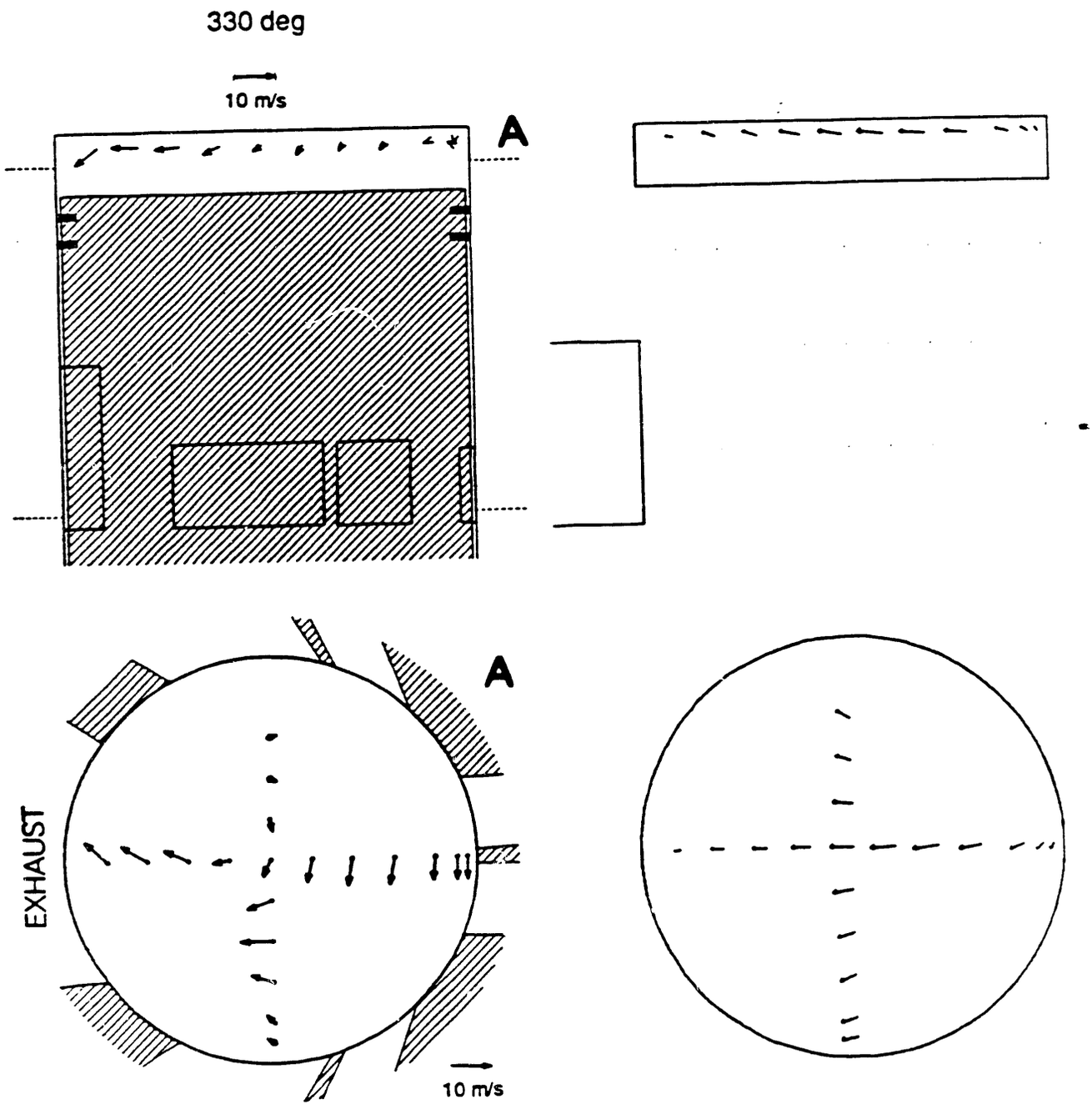

Fig. 6h

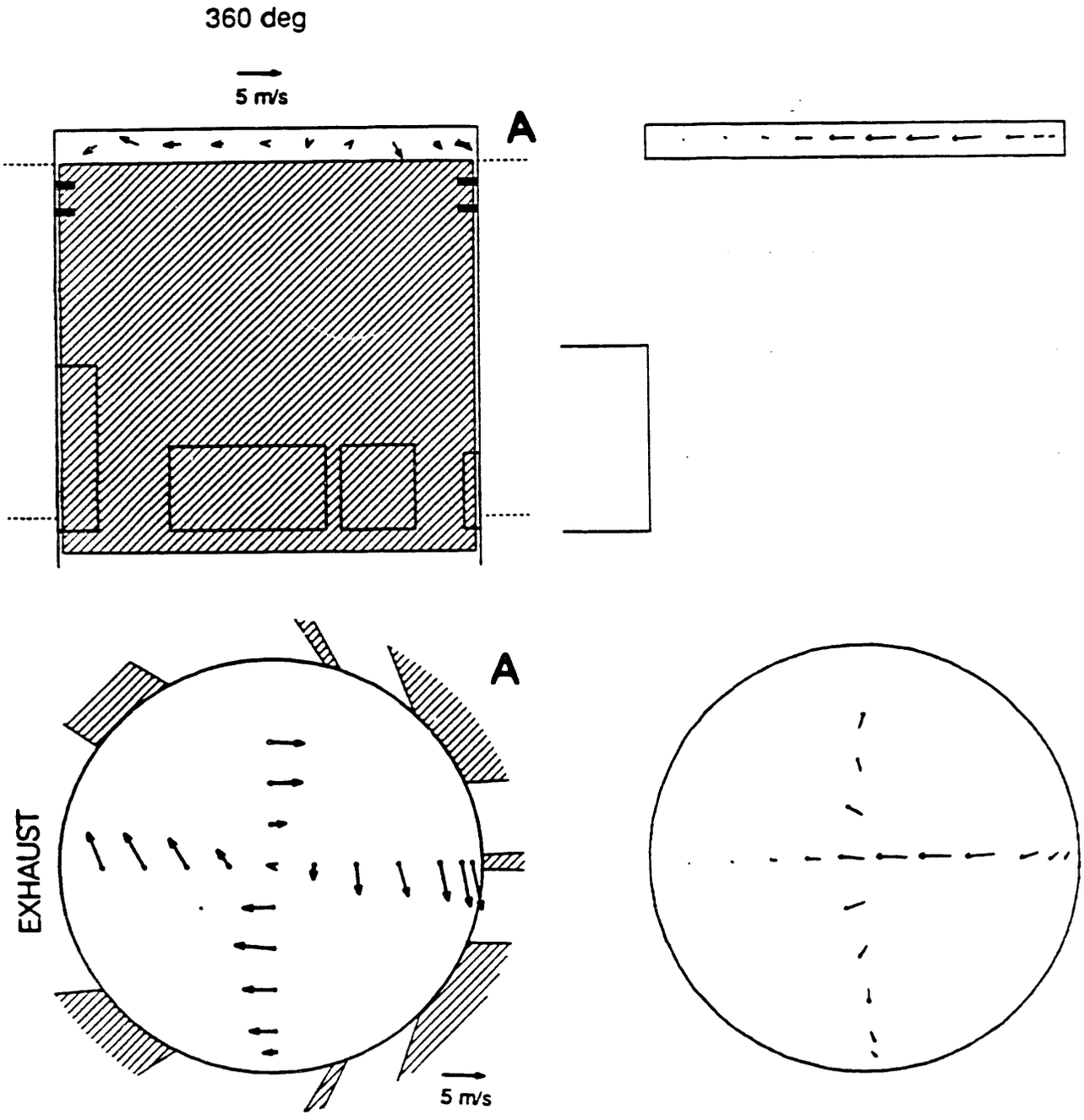

Fig. 6i

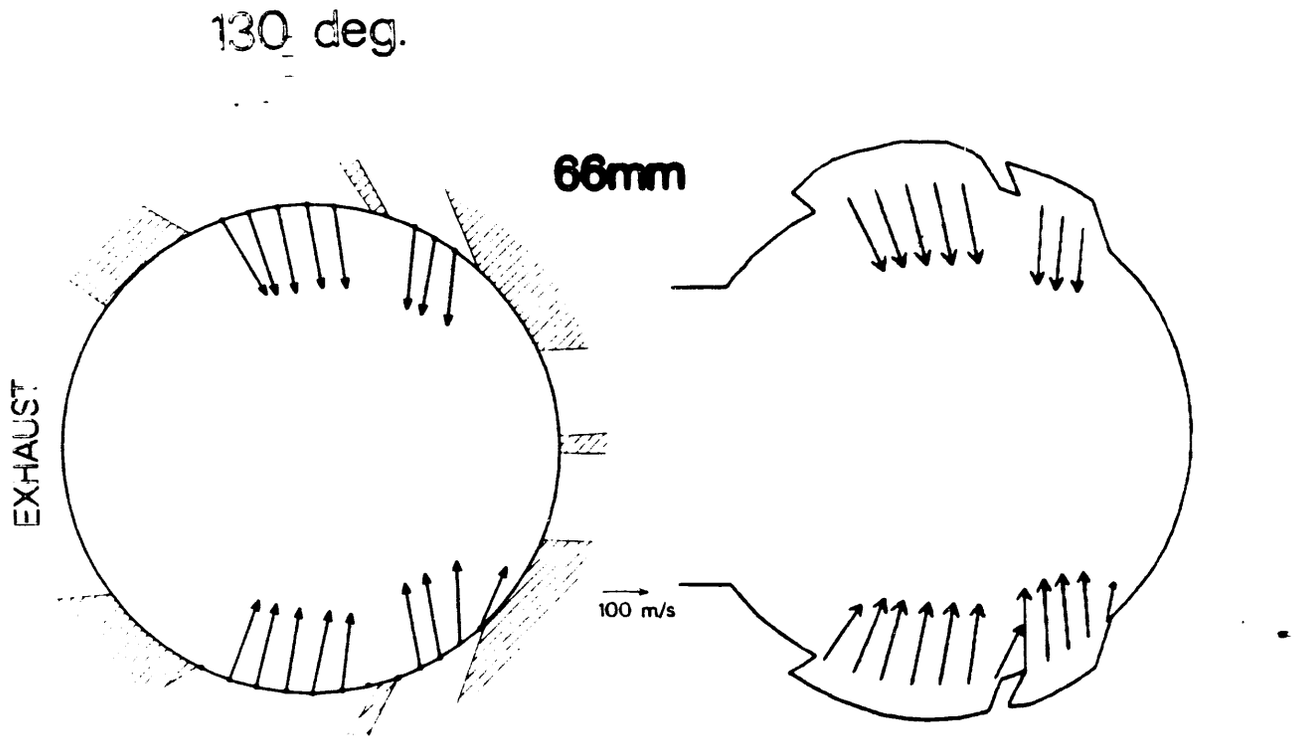

Fig. 7a

135 deg.

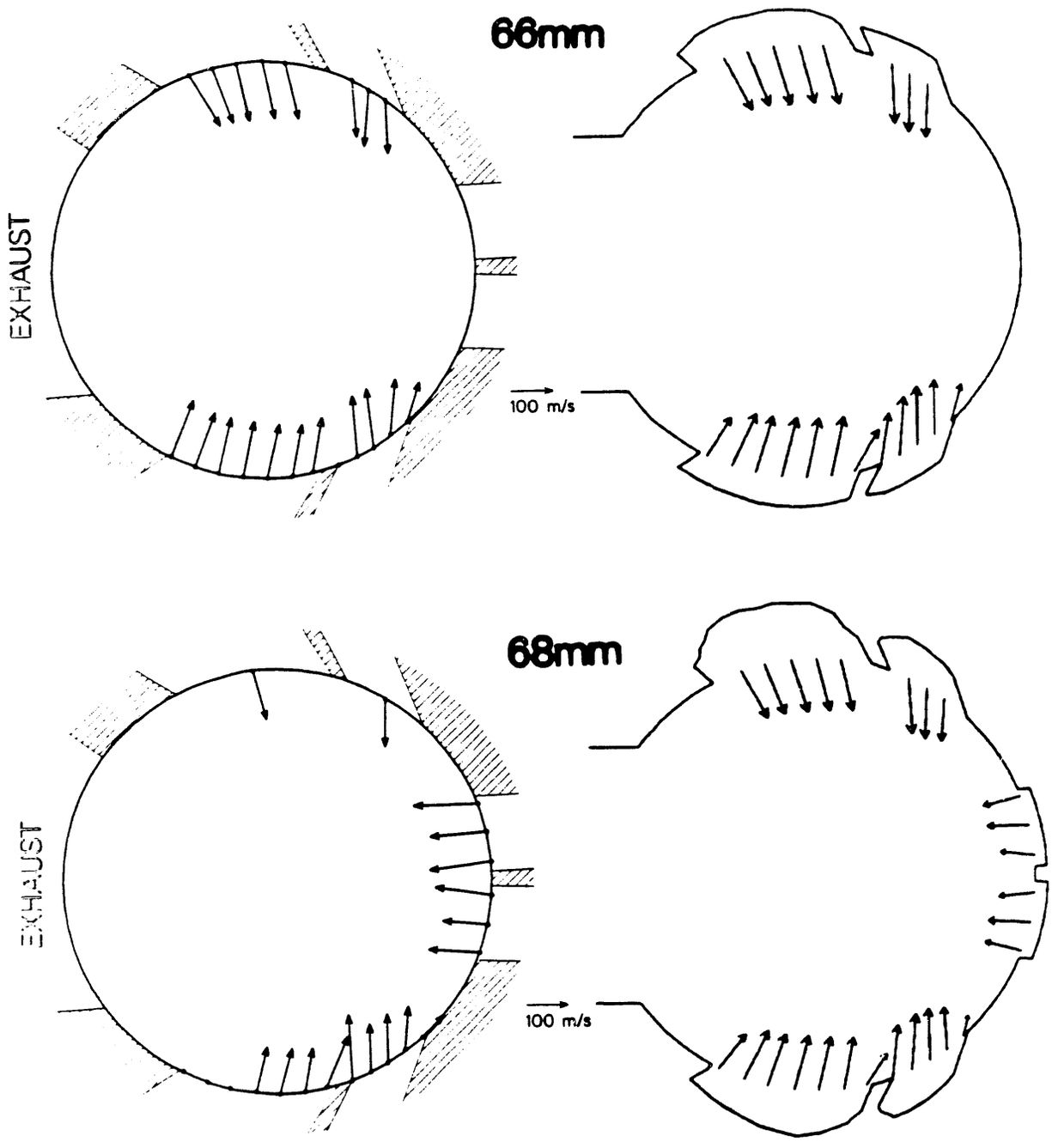

Fig. 7b

140 deg.

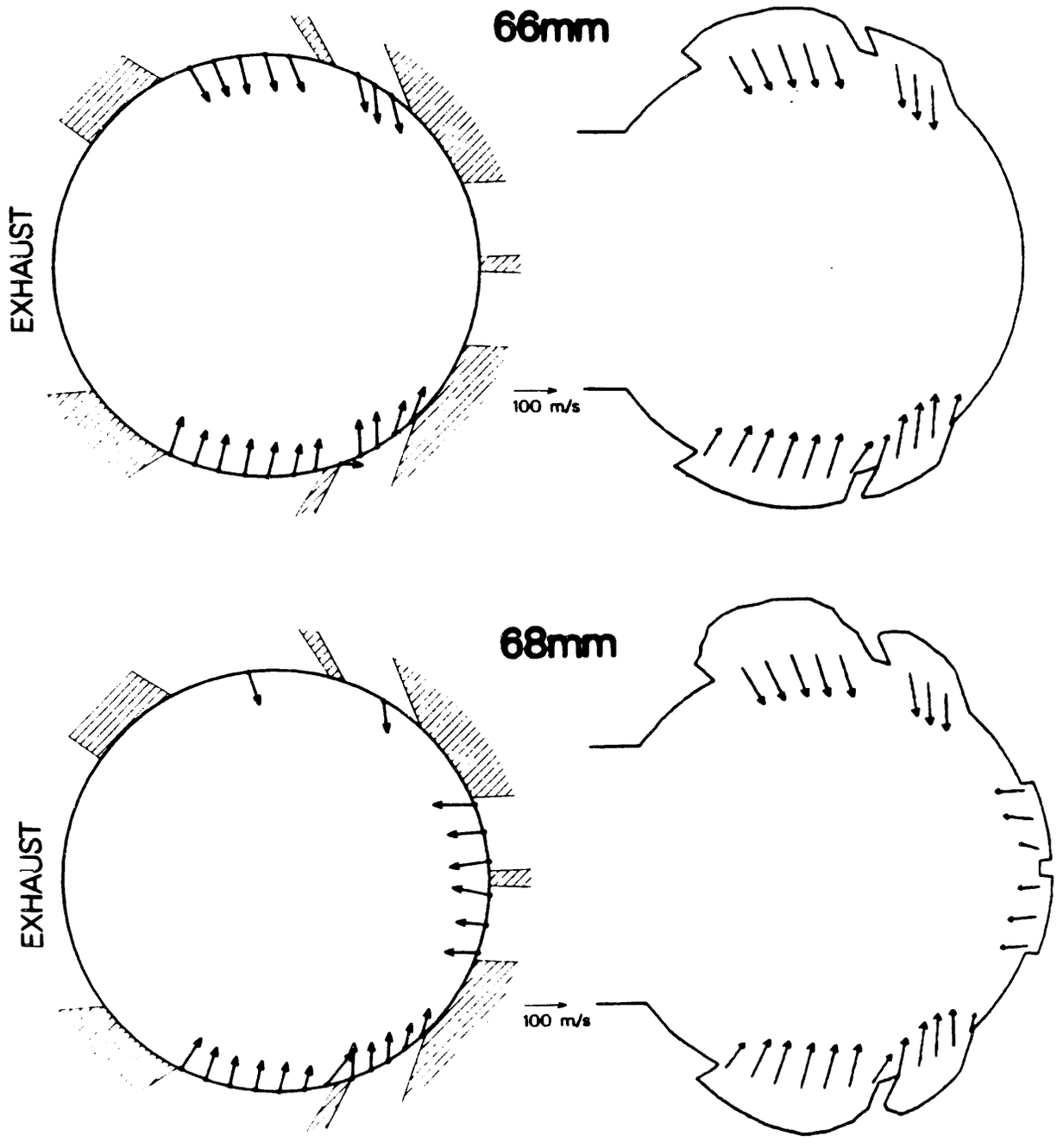

Fig. 7c

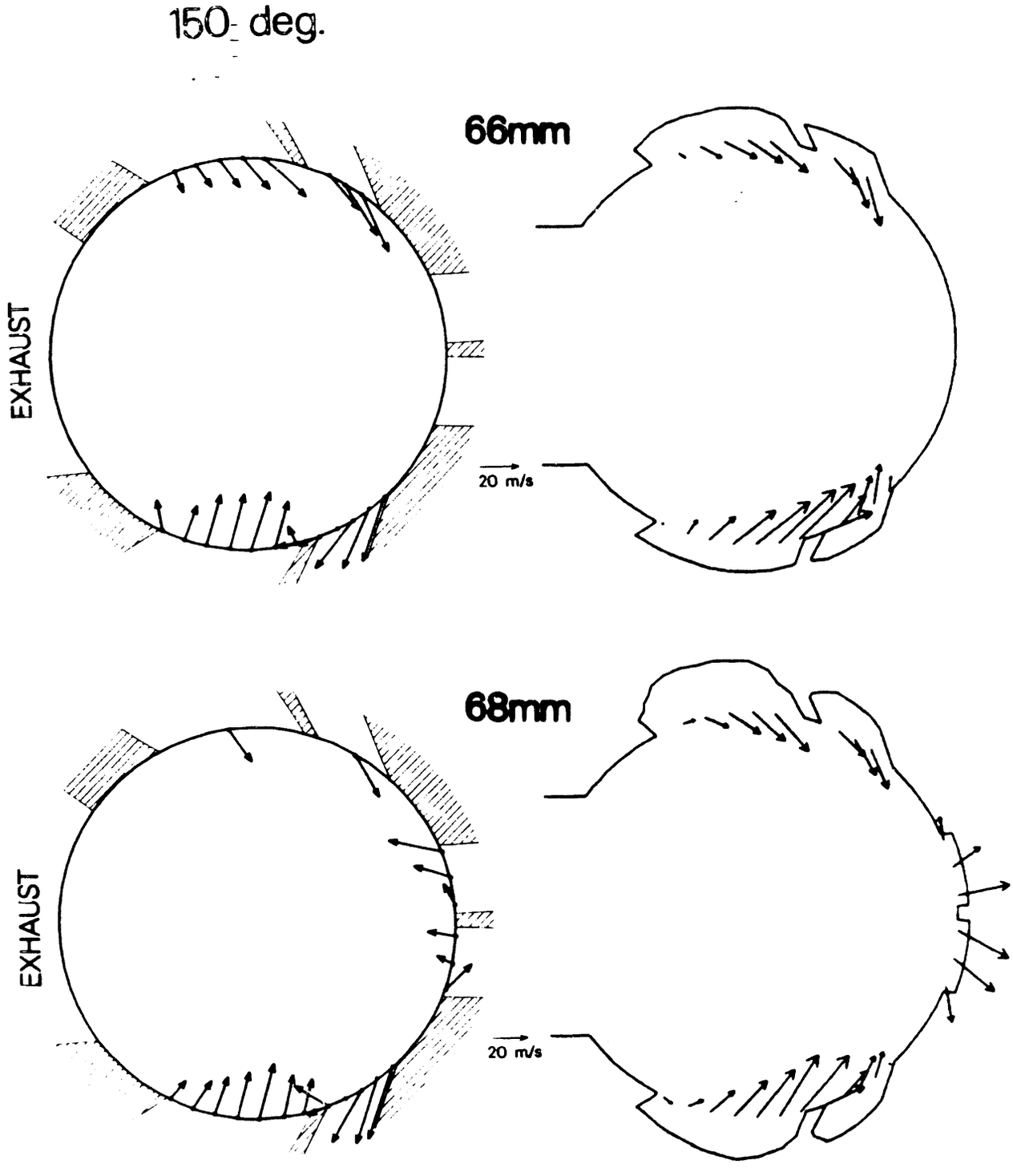

Fig. 7d

END

DATE
FILMED

01/08/92